Regional Contrast of Mesoscale Convective System Structure prior to and during Monsoon Onset across South America

THOMAS M. RICKENBACH, ROSANA NIETO-FERREIRA, AND RICHARD P. BARNHILL*

Department of Geography, East Carolina University, Greenville, North Carolina

STEPHEN W. NESBITT

Department of Atmospheric Sciences, University of Illinois at Urbana–Champaign, Urbana, Illinois

(Manuscript received 5 August 2010, in final form 7 February 2011)

ABSTRACT

In this study, a 10-yr (1998–2007) climatology of observations from the Tropical Rainfall Measuring Mission (TRMM) satellite is used to study regional mechanisms of monsoon onset across tropical and subtropical South America. The approach is to contrast regional differences in the structure, intensity, and rainfall of mesoscale convective systems (MCSs) prior to and after onset, in the context of thermodynamic conditions from the National Centers for Environmental Prediction (NCEP) reanalysis data. This is accomplished by analyzing the mean annual cycle time series, 10-yr frequency histograms, and 3-month-averaged values prior to and following onset in four regions of distinct rainfall variability. Observed MCS metrics and NCEP variables include lightning flash rate, convective rain fraction, height of the 30-dBZ isosurface, minimum 85-GHz polarization corrected temperature, and the fluxes of sensible and latent heat.

The west-central Amazon region had a distinct maximum of MCS intensity 2 months prior to the monsoon onset date of each region, which was well correlated with surface sensible heat flux, despite the observation that thermodynamic instability was greatest after onset. At the mouth of the Amazon, the dry season rainfall minimum, the premonsoon maximum in MCS intensity metrics, and monsoon onset were all delayed by 2–3 months relative to the west-central Amazon. This delay in the annual cycle and comparatively large difference in pre- versus postonset MCSs, combined with previous work, suggest that the slow migration of the Atlantic Ocean intertropical convergence zone controls onset characteristics at the mouth of the Amazon. All metrics of convective intensity in the tropical regions decreased significantly following onset. These results, in the context of previous studies, are consistent with the hypothesis that thermodynamic, land surface, and aerosol controls on MCS intensity operate in concert with each other to control the evolution of precipitation system structure from the dry season to the wet season. The other two regions [the South Atlantic convergence zone (SACZ) and the south], associated with the well-documented dipole of intraseasonal rain variability, have a weaker and more variable annual cycle of all MCS metrics. This is likely related to the strong influence of baroclinic circulations and frontal systems in those regions. In the south, fewer but larger and more electrified MCSs prior to onset transition to more, smaller, and less electrified MCSs after onset, consistent with previous climatologies of strong springtime mesoscale convective complexes in that region.

1. Introduction

While the annual cycle of cloudiness and precipitation across tropical South America has the characteristic summertime maximum of a monsoon climate (Kousky 1988; Horel et al. 1989; Marengo et al. 2001; Gonzalez et al. 2007), the South American monsoon system (SAMS) contains unique and complex features that challenge our understanding of how the monsoon evolves. The onset of the wet season in classic monsoon systems such as in southwestern Asia and northern Australia begins with a reversal of low-level wind direction to onshore flow. In contrast, low-level flow across the SAMS is onshore (easterly) year-round (Zhou and Lau 1998). As monsoon onset approaches, the mean low-level meridional wind component in the tropics becomes northerly, following

* Current affliation: I. M. Systems Group, NOAA/NESDIS, Camp Springs, Maryland.

Corresponding author address: Thomas M. Rickenbach, Department of Geography, East Carolina University, A-227 Brewster Bldg., Greenville, NC 27858-4353.
E-mail: rickenbacht@ecu.edu

DOI: 10.1175/2011JCLI3975.1

the southward migration of solar heating over the continent. This flow is enhanced ahead of frontal systems that extend equatorward from higher latitudes, drawing tropical moisture southeastward in a low-level jet. Combined, these features contribute to the establishment of the South Atlantic convergence zone (SACZ), a hallmark of the mature monsoon (Fu et al. 1999; Liebmann et al. 1999; Garreaud 2000; Rickenbach et al. 2002; Carvalho et al. 2002; Jones and Carvalho 2002; Marengo et al. 2004; Carvalho et al. 2004; Liebmann et al. 2004; Nieto-Ferreira and Rickenbach 2010, hereafter NR10).

In tropical South America, the annual cycle of precipitation is, in the broadest sense, driven by the seasonal migration of solar radiation. In the tropics, thermodynamic instability increases as monsoon onset approaches and remains high during the wet season (Fu and Li 2004; Fisch et al. 2004). Yet, studies suggest that the most vertically intense convective systems occur well before onset during the ''dry'' season (recognizing that most regions in tropical South America experience some rain during the dry season). Increased thermodynamic instability, combined with a high concentration of cloud condensation nuclei (CCN) via biomass burning (Artaxo et al. 2002; Williams et al. 2002) coincide with the deepest, most electrified convective systems 2–3 months prior to monsoon onset in western Amazonia (Petersen and Rutledge 2001). The influence of aerosols from seasonal burning on precipitation efficiency and structure of convective clouds has been well documented (Andreae et al. 2004): an increase in CCN increases the number of smaller cloud drops, allowing more water condensate to reach the upper part of the convective clouds. This lowers precipitation efficiency and enhances updraft strength by the release of latent heat by the freezing of the small drops. The intense premonsoon rain systems contrast with the widespread, rainier, but vertically weaker systems of the monsoon (Petersen and Rutledge 2001; Williams et al. 2002). These studies suggest that a combination of aerosol loading and thermodynamic instability conspire to maximize convective intensity in the ''premonsoon'' period, though the relative importance of these factors are not well understood.

Land surface type also plays an important role in the evolution of the monsoon in that a wetter dry season with enhanced surface moisture flux from a forested surface favors earlier onset (Fu and Li 2004). Seasonal variation in moisture available for precipitation derives in part from seasonal changes in evapotranspiration from the forested canopy (Salati and Vose 1984). As the monsoon begins across the continent, the Atlantic intertropical convergence zone (ITCZ) migrates southward more slowly than the inland ITCZ, which delays onset at the mouth of the Amazon River compared to the interior (Marengo et al. 2001; NR10).

The focus of the present study is to use long-term observations from space to examine regional differences in the structure and intensity of precipitation systems prior to and after monsoon onset. A better understanding of the seasonal transition to onset in key regions will help to evaluate distinct regional mechanisms controlling onset in the SAMS. The regions are objectively defined, chosen based on distinct variability of the annual cycle of rainfall as described in NR10. We examine the annual cycle of the structure and rainfall of mesoscale convective systems (MCSs) in regions of distinct annual variability. We construct a 10-yr (1998–2007) climatology of MCS observations from the Tropical Rainfall Measuring Mission (TRMM) satellite to examine regional differences in convective system structure and intensity during the annual cycle across tropical South America, focusing on the period leading up to and following monsoon onset. We then contrast the mean dry-to-wet season evolution of MCS structure in these regions, and from these observations evaluate onset mechanisms that operate in each region. Section 2 describes the datasets and analysis techniques used, sections 3 and 4 present results for the four regions, and section 5 offers conclusions.

2. Data and methods

This study builds on the regional analysis of monsoon onset described in NR10. A rotated empirical orthogonal function (REOF) analysis of version 2 of the Global Precipitation Climatology Project (GPCP-v2) precipitation data presented in NR10 suggested four regions of distinct annual variability of precipitation in the SAMS region (Fig. 1). The first two REOFs represent independent modes of annual precipitation variability located in the west-central Amazon (region I, 14.1% of the variance explained) and the mouth of Amazon (region II, 12.9% of the variance explained) indicated in Fig. 1. The third REOF (8.1% of the variance) captures the well-known dipole of rain variability in the wet season (Nogues-Paegle and Mo 1997), denoted as region III (SACZ) and region IV (the south) in Fig. 1. NR10 described and used an objective methodology to identify the monsoon onset pentad (5-day period) in each of 42 total 5° × 5° land ''boxes'' (Fig. 1) across tropical and subtropical South America using the GPCP-v2 (Adler et al. 2003) pentad-averaged precipitation dataset for each year during the period 1979–2007. The onset pentad for each of the four regions was determined by the average of the onset pentads for the 5° boxes within each region. As discussed in NR10, the determination of onset date is sensitive to the methodology, dataset, and averaging period. NR10 present a range of onset pentads, based on analysis of different precipitation datasets from several previous studies, of

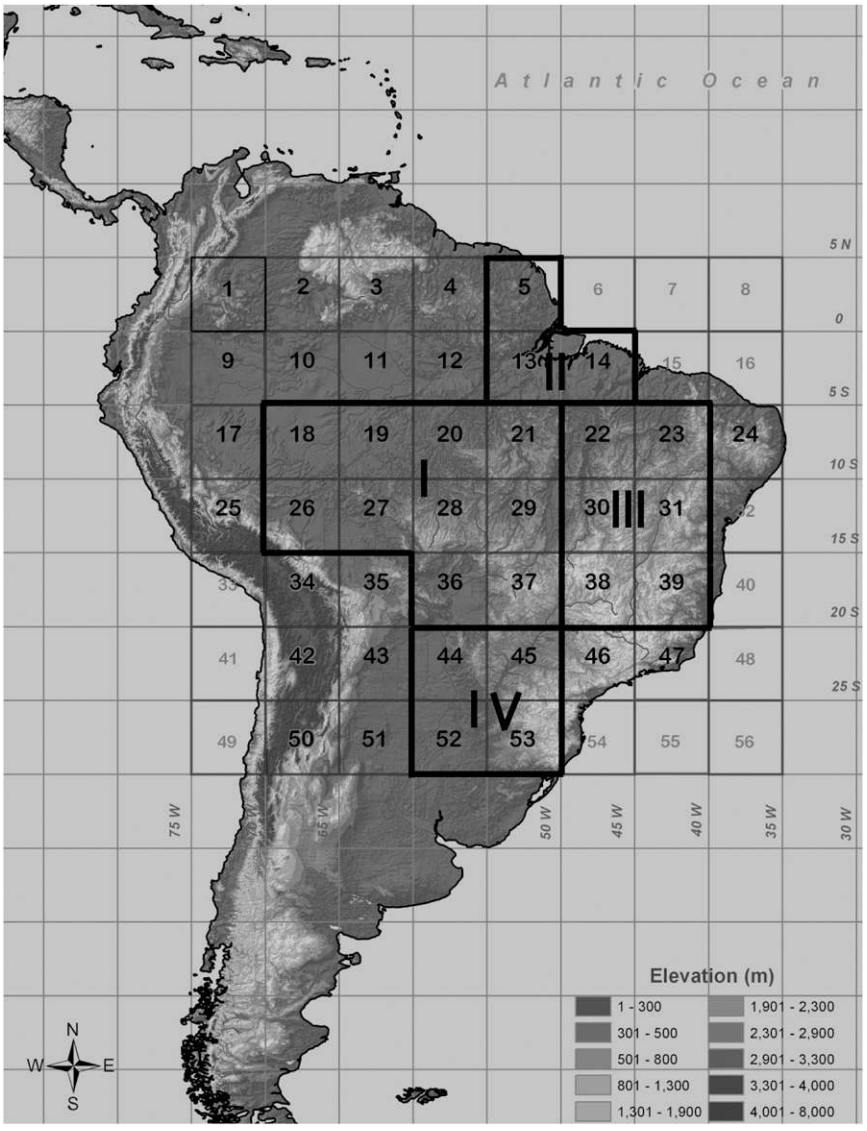

FIG. 1. The SAMS domain divided into 5° × 5° land boxes (boldface numbers) and analysis regions (roman numbers) based on the first three REOFs of the GPCP-v2 pentad precipitation data. The regions are I: west-central Amazon, II: mouth of the Amazon, III: SACZ, and IV: the south.

between 56 and 63 for a region similar to region I (Fig. 1). The present study used an onset pentad of 60 for that region, determined by NR10, which falls in the middle of the range of onset pentads from previous studies. The main conclusions of this paper would not change if any onset pentad in that range were used, thus uncertainties in the determination of onset date do not fundamentally affect these results. The same conclusion holds for onset pentads in the other regions shown in Fig. 1.

Metrics of rainfall, intensity, and organization of precipitating systems were extracted from the TRMM satellite Precipitation Feature Data Base (PFDB; Nesbitt et al. 2000, 2006). A precipitation feature (PF) represents a contiguous portion of an MCS or smaller group of precipitating clouds identified from the TRMM precipitation radar during each overpass. Each PF is classified into one of three categories of organization and vertical structure (Nesbitt et al. 2000) using thresholds of TRMM Precipitation Radar reflectivity and TRMM Microwave Imager polarization-corrected brightness temperature (PCT) at 85 GHz. Scattering of upwelling microwave radiation at this frequency by large ice particles in the upper portion of convective clouds results in low 85-GHz PCT, suggestive of strong convection (Mohr and Zipser 1996). The

first category includes PFs that satisfy the size definition of an MCS (rain area $\geq$ 100 km in maximum elliptical dimension; Houze 1989) and contain an ice scattering signature (minimum 85-GHz PCT $<$ 250 K) indicative of deep convective updrafts and strong convection. The present analysis focuses on the MCS category, since MCSs produce the majority of tropical rainfall in general (Nesbitt et al. 2000) and South American rainfall in particular (Zipser et al. 2006; Durkee et al. 2009). The second category contains smaller PFs with an ice scattering signature that do not meet the rain area threshold of an MCS and are interpreted as deep convective clouds. The third category is defined as those smaller PFs without an ice scattering signature, representing isolated, shallow convection. A regional analysis of the two smaller PF categories will be the subject of a forthcoming paper.

Observational metrics derived for each PF include rain rate, raining area, convective (vs stratiform) rain fraction, the vertical structure of radar reflectivity, minimum 85-GHz PCT, and lightning flash rate. The convective rain fraction is the fraction of the rain that is associated with active convective cells, in contrast with lighter, homogeneous stratiform rain (Houze 1989). The last three metrics are proxies for the intensity of vertical air motions within convective cells (the term ''intensity'' is used hereafter with regard to the vertical development of convection). The maximum height of the 30-dBZ isosurface in each PF has been identified in previous studies (DeMott and Rutledge 1998; Petersen and Rutledge 2001; Nesbitt et al. 2006) as a useful measure of the vertical intensity of convective systems. Larger values of this parameter indicate the presence of stronger updrafts lofting more water condensate to higher altitudes (Zipser and Lutz 1994). Lightning flash rate is positively correlated with the strength of vertical air motions within a storm (Williams et al. 1989), and therefore provides an independent measure of the vigor of convective updrafts. Low values of minimum 85-GHz PCT represent another independent metric of deep convection (as discussed earlier).

The PF metrics described above were averaged over each of the 5° boxes for each pentad from 1998 through 2007 and then averaged over each of the four analysis regions shown in Fig. 1. The 5-day averages were taken to ensure sufficient sampling for robust estimates of each parameter. The pentad data were used to construct time series of the mean (1998–2007) annual cycle for each parameter, and to compile frequency histograms for the 10-yr period.

The National Centers for Environmental Prediction (NCEP) reanalysis dataset (Kalnay et al. 1996) is used to characterize the annual cycle of the regional thermodynamic environment. The PF time series for each of the four regions are analyzed along with thermodynamic fields from the NCEP reanalysis. We focus on surface energy exchange with the atmosphere via time series of sensible and latent heat flux, and on the thermodynamic stability of the troposphere using time–height diagrams of the vertical profile of equivalent potential temperature. Thermodynamic instability can be qualitatively represented by the vertical gradient of equivalent potential temperature (Holton 2004). We chose not to derive convective available potential energy (CAPE) from the NCEP reanalysis as a measure of thermodynamic instability because of the strong dependence of CAPE on the choice of boundary layer parcel to lift, combined with the poor vertical resolution of the NCEP fields in and above the boundary layer.

3. Climatology and annual cycle: Regions I–IV

The 1998–2007 climatology of rainfall, lightning flash rate, minimum 85-GHz PCT, and maximum height of the 30-dBZ isosurface (Fig. 2), presented as frequency histograms for each of regions I–IV (cf. Fig. 1), provide the general context to study the evolution of regional differences in the structure and rainfall of MCSs leading up to monsoon onset.

The TRMM PF 10-yr rainfall climatology was consistent with other independent satellite precipitation climatologies for South America discussed in NR10. In the deep tropics (regions I–III), the upper tail of the distribution of rainfall rate (Fig. 2a) was shifted more to higher values in region I (west-central Amazon), region II (mouth of the Amazon) had a narrower distribution centered at weaker rainfall, and region III (SACZ) was intermediate. NR10 pointed out that the Atlantic ITCZ intersects region II (mouth of the Amazon), suggesting a geographic linkage between the oceanic ITCZ and rainfall in that coastal region. Oceanic convection in the tropics is generally weaker in updraft strength, shallower in vertical reflectivity structure, and lower in lightning flash rate than tropical land-based convection (Zipser et al. 2006). Compared to the other regions, the region II (mouth of the Amazon) frequency distribution of the convective intensity metrics of lightning flash rate, minimum 85-GHz PCT, and 30-dBZ height (Figs. 2b–d) were each shifted to values indicating weaker convection, consistent with the influence of an oceanic regime there. Region I (west-central Amazon) and region III (SACZ) were similar in the distributions of lightning flash rate and the ''cold'' tail of the minimum 85-GHz PCT, suggesting active ice processes in the upper troposphere in both regions. The upper tail of the 30-dBZ height distribution of region III was shifted to deeper convection compared to region I, consistent with the greater instability and sensible heat flux in region III (see section 3). The general similarity of regions I and III was consistent with previous

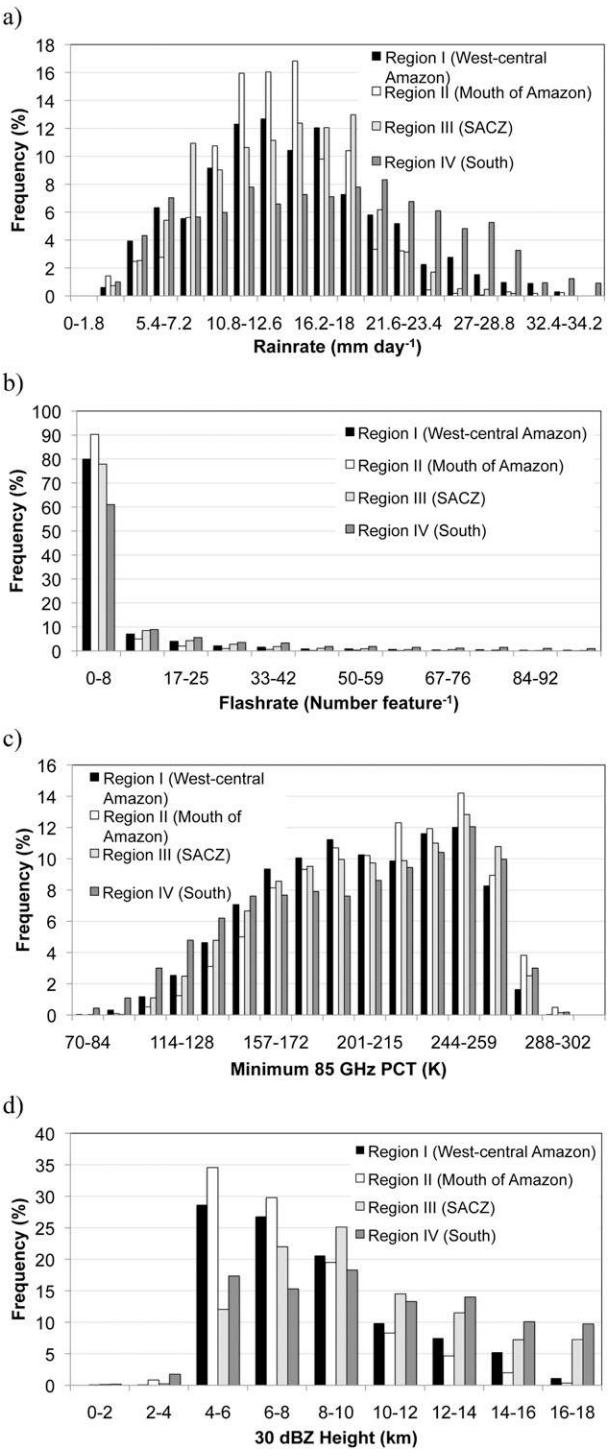

FIG. 2. Frequency histograms (1998–2007) for regions I–IV of TRMM-observed MCS feature parameters of (a) rainfall rate (mm day^{-1}), (b) lightning flash rate (number per feature), (c) minimum 85-GHz polarization corrected temperature (K), and (d) height (km) of the 30-dBZ isosurface.

studies that have suggested that these two regions are linked, as the low-level jet transports moisture from region I to region III contributing to the formation of the SACZ (Liebmann et al. 1999; Carvalho et al. 2002, 2004; Jones and Carvalho 2002; Marengo et al. 2004; Liebmann et al. 2004; Rickenbach et al. 2002). Figure 2 illustrates that the heaviest rainfall and most intense MCSs by all measures (lightning, ice scattering, and depth) occurred in the subtropics in region IV (the south) compared to the other regions. Region IV has been associated with large MCSs and the larger, more persistent mesoscale convective complexes (MCCs), which are most common during the spring and continue in the summer months (Velasco and Fritsch 1987; Durkee and Mote 2009). Previous studies (Christian et al. 2003; Zipser et al. 2006) associate metrics of intense convection from TRMM with the seasonal MCSs and MCCs in that region, consistent with the TRMM PFDB results shown here.

We now contrast the 1998–2007 mean annual cycle of MCS rainfall, lightning flash rate, convective rain fraction, and maximum 30-dBZ height, along with the fluxes of sensible and latent heat and profiles of equivalent potential temperature, in each of the four regions (Figs. 3–6). The minimum 85-GHz PCT is not shown, since the annual cycle is not pronounced. Each of the TRMM metrics has been smoothed with a seven-point central moving average to reduce higher-frequency variations associated with the relatively short (10 yr) average.

a. Region I (west-central Amazon)

The REOF analysis of GPCP precipitation data by NR10 determined that, of the four regions, region I (west-central Amazon) explained the most variance in the rainfall annual cycle over South America. The TRMM PF annual cycle of MCS rainfall along with MCS intensity parameters for region I are shown in Fig. 3a. Following the rainfall minimum in early June, all metrics of system intensity (lightning, convective rain fraction, 30-dBZ height) increased together to a general maximum from late July through August (pentads 41–48). These observations indicate that convection associated with premonsoon MCSs was more vertically developed than during the wet season. The annual maximum in MCS intensity occurred fully 2 months prior to monsoon onset in region I. Strong convection has been noted by Petersen and Rutledge (2001) in September–November for an area similar to this region, though their study did not examine July–August. Sensible heat flux increased from June to a maximum in mid-August, in step with the metrics of system intensity. The annual cycle of sensible heat flux and lightning flash rate were particularly well correlated (correlation coefficient of 0.94). Latent heat flux decreased during the dry season to a mid-August minimum. Thus, the maximum in

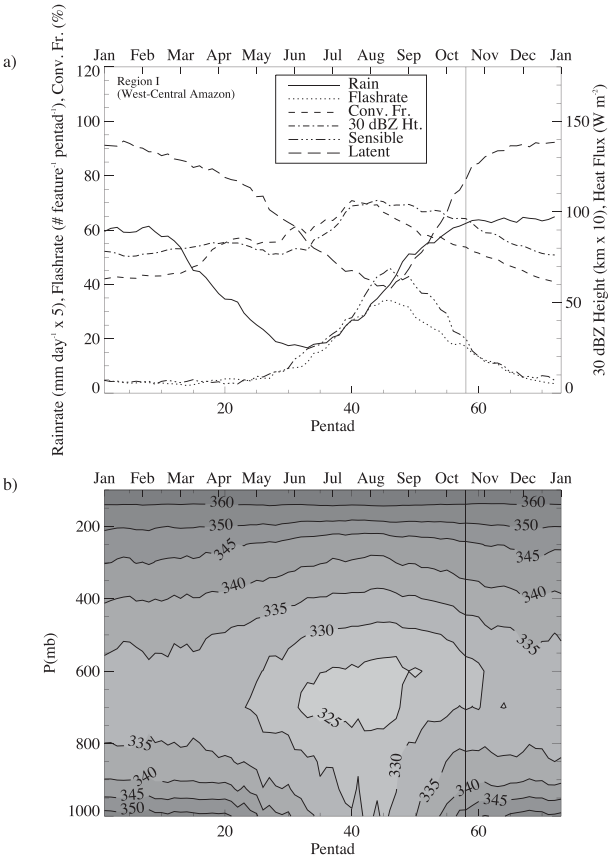

FIG. 3. The 1998–2007 mean annual cycle for region I (west-central Amazon) of TRMM MCS feature metrics and NCEP reanalysis parameters for (a) MCS rain rate (mm day^{-1} × 5, solid), MCS lightning flash rate (number per feature per pentad, dotted), MCS convective rain fraction (%, short dashed), MCS height of the 30-dBZ isosurface (km × 10, dashed-single dot), NCEP reanalysis sensible heat flux (W m^{-2}, dashed-three dots) and latent heat flux (W m^{-2}, long dashed); (b) vertical profile of equivalent potential temperature (K). The TRMM parameters have been smoothed using a seven-point central moving average. Vertical solid lines indicate the mean onset pentad for that region.

convective intensity 2 months before onset coincided with a seasonal maximum in the Bowen ratio (sensible heat divided by latent heat), which slightly exceeded unity from late July through August. Following this maximum, sensible heat decreased and latent heat increased in the 2 months leading up to monsoon onset, associated with the seasonal increase in surface temperature and specific humidity. For the 2 months approaching monsoon onset, all metrics of system intensity decreased. MCSs became less convective with decreasing vertical intensity and lightning even as MCS rainfall increased up to a mid-October onset.

The annual cycle of the vertical profile of equivalent potential temperature (Fig. 3b) indicated that thermodynamic instability, inferred from the vertical gradient of potential temperature between the surface and 700 mb, was greatest in the wet (summer) season, associated with the increased seasonal heating and moistening of the lower troposphere. The higher instability of the monsoon, also noted in a radiosonde analysis over western Amazonia (Fisch et al. 2004), is quite consistent with the annual cycle of rainfall. Yet, the vertical intensity (lightning and maximum 30-dBZ height) of MCSs was greatest in August at the seasonal minimum of thermodynamic instability in the lower troposphere. In fact, as lower-tropospheric thermodynamic instability increased between August and November, system vertical intensity decreased steadily. We will explore this question next.

The strong correlation between surface sensible heat flux and lightning flash rate suggests that surface energy exchange drives the premonsoon maximum in MCS vertical intensity in August. Fu et al. (1999) concluded from sounding data in the central Amazon basin that high values of convective inhibition in the wintertime (associated with a low-level temperature inversion driven by a cool winter boundary layer) begin to decrease in August coincident with increasing surface sensible heat flux, setting the stage for deeper convection. At the same time, studies show observational evidence that an aerosol mechanism to enhance the strength of convection operates in the Amazon. In the central Amazon, Andreae et al. (2004) documented increased vigor of convection after the clouds ingested smoky air. Increasing CCN from dry season biomass burning leads to more cloud droplets reaching the freezing level in convective updrafts. The resulting energy released by the latent heat of freezing is hypothesized to increase convective system vertical intensity (as described in Williams et al. 2002). Observations of aerosol concentration for a 9-yr period at Alta Floresta, Brazil (near the center of region I) indicate a clear and consistent annual maximum in August associated with biomass burning (Artaxo et al. 2002), coinciding with the present result of the timing of the annual maximum in lightning flash rate, 30-dBZ height, and convective rain fraction (Fig. 3a). Studies of the geographic distribution of aerosols from seasonal burning across tropical South America (Cooke and Wilson 1996; Potter et al. 2001) show that region I includes the greatest concentration of aerosols in the SAMS region. The close association of sensible heat flux and lightning flash rate is consistent with the observations of Fisch et al. (2004) that a deforested surface in the dry season has a factor of 2 larger surface sensible heat flux. In this context, the seasonal change of land surface properties and soil moisture leads to the strong premonsoon maximum in sensible heat flux.

Region I results suggest that thermodynamic priming by increasing surface sensible heat flux is consistent with the maximum in MCS intensity in August, which we will

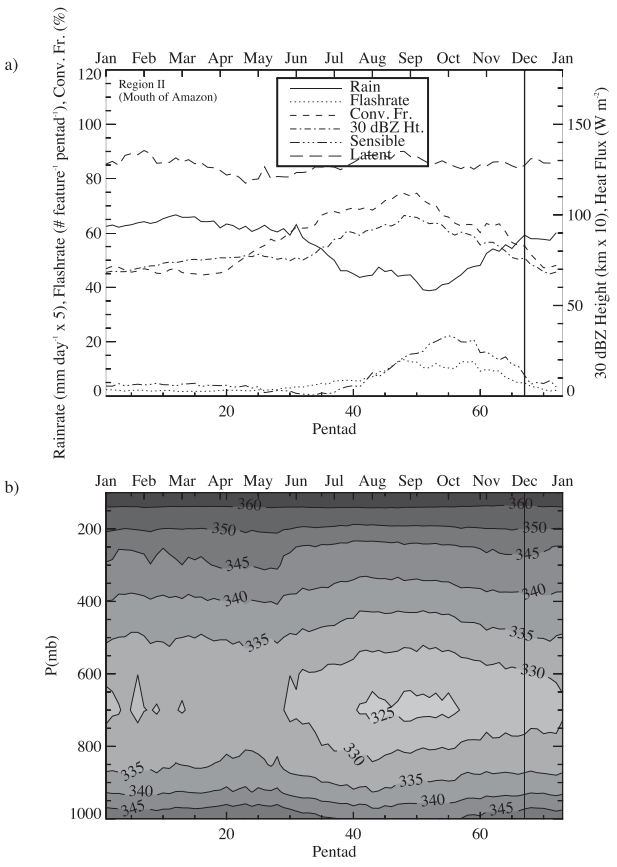

FIG. 4. As in Fig. 3, but for region II (mouth of the Amazon).

discuss further in section 3b. It is important to point out that thermodynamics are not the only control over the formation and structure of MCSs. Squall-line MCSs form in an optimum environment of thermodynamic instability and low-level wind shear (Keenan and Carbone 1992).

b. Region II (mouth of the Amazon)

The annual cycle of rainfall in region II (mouth of the Amazon) differed from region I (west-central Amazon) in two important respects. First, the summer-to-winter difference in the annual cycle of rainfall (Fig. 4a) was considerably weaker, with the peak-to-peak amplitude about 25% less than in region I. Second, the dry season minimum occurred in late September, fully 3 months following that of region I. Both of these observations are consistent with the strong influence of the Atlantic ITCZ in region II discussed earlier. Easterly winds bring oceanic air to region II (Zhou and Lau 1998), leading to a nearly constant surface latent heat flux year-round (Fig. 4a) and contributing to a less pronounced seasonal cycle of rainfall. The delayed dry season and subsequent late monsoon onset date of early December are associated with the slower seasonal migration of the Atlantic ITCZ compared to rainfall over the continent, related to the greater thermal inertia of the ocean (NR10). Accordingly, the thermodynamic instability, as inferred from the vertical profile of equivalent potential temperature (Fig. 4b), had a weaker annual cycle than for region I, with larger instability in the wet season consistent with the annual cycle of rain. The dry season minimum in equivalent potential temperature at 700 mb extended into October, about a month later than for region I. As with region I, there was a well-defined maximum in sensible heat flux 2 months prior to monsoon onset that corresponds well to the annual maximum in lightning flash rate (0.54 correlation coefficient). However, both the sensible heat flux and lightning flash rate maxima were about half as large, and occurred about 2 months later, compared to region I. The convective rain fraction and maximum 30-dBZ height were also largest near the rainfall minimum of early–mid-September, but compared to region I these metrics of convective intensity (including lightning flash rate) were much more variable and also weaker.

Do the results for region II (mouth of the Amazon) shed light on the mechanisms controlling stronger premonsoon convection discussed in the previous section? The thermodynamic observations for region II discussed above, combined with previous studies of the aerosol conditions in this region, are both consistent with weaker MCS intensity and a delay in the timing of the annual intensity maximum compared to region I (west-central Amazon). Observations of aerosols from biomass burning in the dry season presented in Freitas et al. (2005) demonstrate that air in region II is ''cleaner'' than in the central Amazon, because of fewer sources and more pristine (low CCN concentration) oceanic onshore winds. That study further showed the dry season maximum in total carbon mass emitted from combustion at the mouth of the Amazon (October) was delayed by 2 months compared to the west-central Amazon (August). Both of these results are consistent with the present finding of a weaker premonsoon maximum in MCS intensity with a 2-month delay in region II (October) compared to region I (August). It is important to note that the timing of prescribed burning in both regions is engineered to coincide with the timing of the rainfall minimum in the dry season, so these are not strictly independent phenomena.

c. Region III (SACZ)

The timing of the dry season minimum and monsoon onset date in region III (SACZ) was similar to region I (west-central Amazon), though with less average rainfall. However, the annual cycle of rain and of the intensity metrics (Fig. 5a) were more variable (even after smoothing), likely due to rain variations strongly tied to the

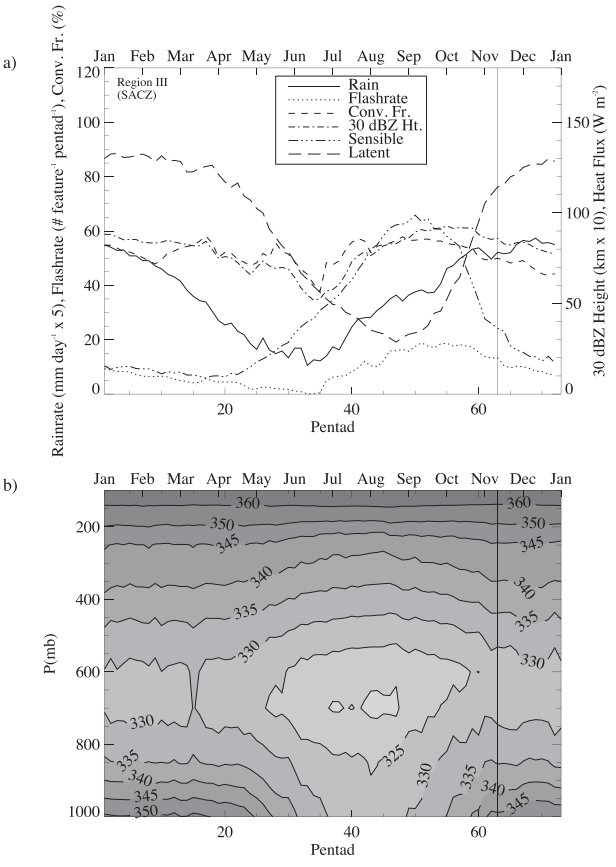

FIG. 5. As in Fig. 3, but for region III (SACZ).

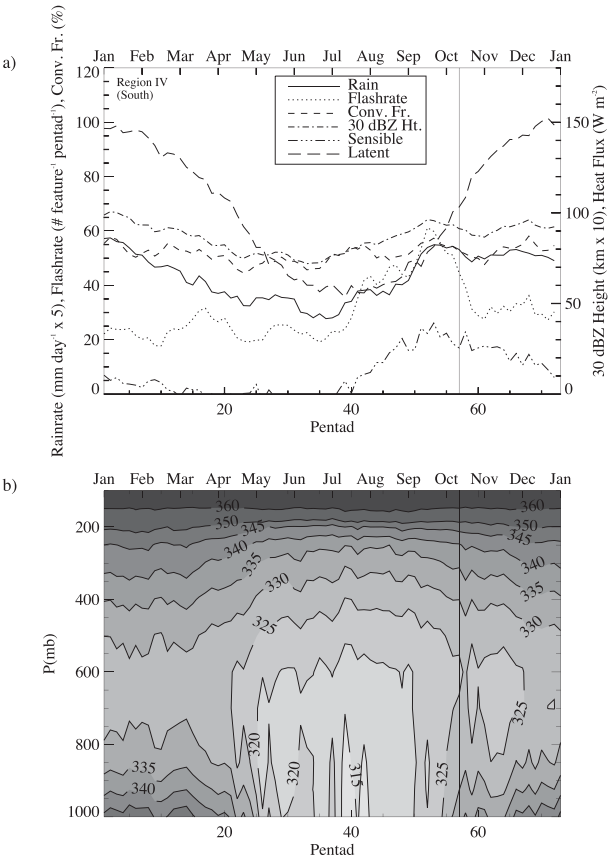

FIG. 6. As in Fig. 3, but for region IV (the south).

passage of transient midlatitude baroclinic wave systems. The lightning flash rate was greater between August and October (premonsoon), though with less of a clear maximum in timing compared to regions I–II. The convective rain fraction and maximum 30-dBZ height also decreased somewhat following onset, but not as dramatically as in region I.

Although the peak in convective intensity metrics of MCSs generally coincided with the seasonal peak in sensible heat flux as in region I, intensity metrics were by comparison weaker in the 3 months prior to onset. The Bowen ratio reached an annual maximum of about 2.5 in late September, twice as large as for region I, although MCS intensity was somewhat weaker than region I. The annual cycle of equivalent potential temperature profiles (Fig. 5b) was very similar to region I in magnitude and timing. The similar evolution of MCS rainfall and intensity from dry to wet season in regions I and III were consistent with the conclusions of NR10 that onset in the west-central Amazon influences the establishment of the SACZ via moisture transport to the SACZ region in a low-level jet ahead of frontal regions, consistent with Liebmann et al. (2004) and Carvalho et al. (2004).

d. Region IV (the south)

The annual variability of region IV (the south) rainfall and intensity metrics (Fig. 6a) were the noisiest of all the regions, due to the influence of wintertime baroclinic systems and the lack of a strong annual cycle. In the context of previous studies, these results suggest that the monsoon precipitation in region IV was dominated by the MCCs common to this region. MCCs are essentially large, long-lived, inertially stable MCSs (Maddox 1980; Cotton et al. 1989) that are associated with baroclinic wave passages (Laing and Fritsch 1997). Each year, these systems bring severe weather and regional flooding to Argentina (Velasco and Fritsch 1987). Large MCC occur with high frequency during the monsoon in this region compared to regions I–III (Durkee and Mote 2009). The climatological monsoon onset date of mid-October in region IV (Fig. 6) coincided with the initial seasonal increase in MCC occurrence documented by Durkee and Mote (2009).

The peak lightning flash rates for several pentads following onset was more than twice as high in region IV than in the other regions. Those results are consistent with the observation of highly electrified MCCs unique to

TABLE 1. The 1998–2007 mean values of pentad averaged MCS intensity and size metrics and Bowen ratio (ratio of sensible to latent heat flux) for 3 months before and 3 months after monsoon onset in each of the four regions. Lightning flash units are number per feature per pentad. The percentage change in each parameter from before to after onset is given in parentheses. Before vs after onset changes in italics are significant to greater than the 95% confidence level using a Student's *t* test, while those in boldface are significant to greater than the 99% confidence level.

	Region I		Region II		Region III		Region IV	
	Before	After	Before	After	Before	After	Before	After
Bowen ratio	*0.76*	*0.097 (−87%)*	*0.20*	*0.049 (−76%)*	*1.9*	*0.16 (−92%)*	**0.30**	**0.15 (–50%)**
Lightning flash rate	*25.4*	*8.1 (−68%)*	**10.2**	**1.5 (–85%)**	**16.8**	**8.6 (–49%)**	**45.1**	**29 (–36%)**
Max 30-dB*Z* height (km)	*10.3*	*8.2 (−20%)*	*8.8*	*7.0 (−20%)*	8.8	8.3 (−6%)	8.7	9.2 (+6%)
Convective rain fraction	*57*	*46 (−19%)*	*64*	*47 (−27%)*	**55**	**49 (–11%)**	53	54 (+2%)
No. of pixels per MCS feature	**426**	**516 (+21%)**	**335**	**423 (+26%)**	*451*	*491 (+9%)*	**532**	**376 (–29%)**
No. of MCS features	*9.0*	*25.3 (+183%)*	*2.0*	*8.1 (+305%)*	*5.6*	*11.2 (+100%)*	*4.0*	*5.8 (+45%)*

that region (Zipser et al. 2006). The wintertime equivalent potential temperature profile (Fig. 6b) was particularly variable, likely associated with the strong variability introduced by baroclinic wave activity. However, as in the tropical regions, there was a summertime increase in thermodynamic instability as inferred from the equivalent potential temperature profiles, consistent with the conditions required for MCC formation in this region (Laing and Fritsch 1997).

4. Mean MCS metrics before and after onset for each region

Table 1 summarizes for each region the change in several metrics of MCS structure and intensity, along with the Bowen ratio, averaged for 3 months prior to and 3 months following each region's monsoon onset pentad. In addition to lightning flash rate, maximum 30-dB*Z* isosurface height, and convective rain fraction, the area (measured here by the number of raining pixels) of the mean MCS feature and the mean number of MCS features are presented.

A common feature of all 4 regions is the significant decrease (to greater than a 95% confidence level according to a Student's *t* test) in lightning flash rate and Bowen ratio in the transition to onset. The average number and area of MCS features in all regions increased significantly after onset. Combined, these changes mean that there are more, larger, and weaker MCSs after onset everywhere in the SAMS. The exception to this was a significant decrease in MCS area after onset in region IV (the south), suggesting that the springtime MCSs in that region were larger than during the summer. The change in pre- to postonset MCS intensity was greatest in regions I and II, with a decrease in postonset lightning by roughly three-fourths, a one-fifth decrease in maximum 30-dB*Z* height and a one-fourth decrease in convective rain fraction (all statistically significant). The greatest difference in all metrics of pre- to postonset MCS intensity, size, and number occurred between regions II and I, suggesting that the oceanic influence at the mouth of the Amazon more severely curtailed MCS intensity after onset compared to the west-central Amazon. Region III (SACZ) has a comparatively lower pre- to postonset difference in MCS properties, despite a larger drop in the Bowen ratio. In region IV (the south), where the well-studied MCCs occur during the monsoon (October–May), the mean size of MCS features decreased significantly after onset as discussed previously, with a slight increase (not statistically significant) in maximum 30-dB*Z* height and convective rain fraction despite a significant one-third decrease in lightning flash rate. This suggests that in region IV, fewer but larger and more electrified MCSs prior to onset transition to more, smaller, and less electrified MCSs after onset.

5. Conclusions

Regional differences in a 10-yr (1998–2007) climatology of MCS rainfall, intensity, and thermodynamic environment were examined in the context of previous investigations to study the mechanisms involved in the transition from the dry season to monsoon onset in South America. Rainfall, lightning flash rate, vertical radar reflectivity structure, and convective rainfall fraction associated with MCSs were analyzed using data from the TRMM satellite. Surface fluxes of sensible and latent heat and the vertical profile of equivalent potential temperature were examined from the NCEP reanalysis data. Four regions across tropical and subtropical South America were compared. These regions were selected objectively in a prior study based on geographically distinct modes of rainfall variability. Results were placed in the context of previous investigations of the mechanisms controlling the structure of precipitation systems in the transition from the dry to wet season.

Region I (west-central Amazon) and region II (mouth of the Amazon) had the greatest pre- to postmonsoon onset change in rainfall. Metrics related to the vertical

intensity of MCSs showed distinct maxima 2 months before monsoon onset in regions I and II. The timing of the maximum in MCS intensity was different in each region, with the region I maximum in August and a delayed maximum in region II during October. This delay in the annual cycle, combined with much weaker MCS intensity, low Bowen ratio, lack of annual cycle in surface latent heat flux, and proximity to the coast, suggest that the slow migration of the Atlantic ITCZ determines the timing of onset in region II. In both regions, MCS intensity subsequently decreased leading up to and following onset. The changes in pre- to postonset MCS intensity, size, and number were greater for region II compared to region I, suggesting the oceanic influence at the mouth of the Amazon more severely curtailed MCS intensity after onset compared to the west-central Amazon interior.

When placed in the context of the previous studies discussed in section 3, results for regions I and II suggest that thermodynamic, surface energy flux, and aerosol controls on MCS intensity likely operate in concert with each other. As suggested earlier, the surface heating may weaken the wintertime low-level inversion and erode convective inhibition sufficiently for deep convection to grow explosively. At the same time, the coincident timing of maxima in convective intensity metrics (lightning flash rate and 30-dBZ isosurface height) and the general timing of observed seasonal maxima in aerosol concentration (Artaxo et al. 2002) are consistent with the hypothesis that the higher concentrations of CCN during the burning season energizes convection via an increase in latent heat of freezing in the upper levels of the clouds due to a shift to smaller sizes of the cloud drop size distribution (Andreae et al. 2004). Surface sensible heat flux decreases approaching monsoon onset, likely in association with the increase in cloudiness and rainfall, lead to widespread but less vertically intense convection. The increase in rainfall approaching monsoon onset limits aerosol production as the burning is curtailed. This scenario thus envisions a tight coupling between the seasonal changes in aerosol concentrations, surface energy fluxes, and the thermodynamic environment, all of which are interdependent and mutually reinforcing. As such, observational studies alone cannot assess the relative importance of these effects on MCS properties; such an assessment necessarily requires modeling studies.

The other two regions (SACZ and the south), associated with the well-documented dipole of intraseasonal rain variability, have a weaker and noisier annual cycle of all MCS metrics, despite a strong annual cycle in thermodynamic instability. In region IV (the south) the large, highly electrified MCSs just prior to onset are associated with the climatological occurrence of mesoscale convective complexes beginning in October. The large variability and weak annual cycle of MCS metrics in region IV likely stem from the presence of both a wintertime baroclinic rainfall regime and a summertime, thermodynamically driven rainfall regime. The similar evolution of MCS rainfall and intensity from pre- to postonset in region I (west-central Amazon) and region III (SACZ) highlight the connection between these regions. Onset in the west-central Amazon is an important precursor to the establishment of the SACZ via moisture transport to the SACZ region in the low-level jet ahead of fronts. Future work will focus on the year-to-year variation of these trends, with an analysis of the annual cycle and frequency distributions of smaller (non MCS) precipitation features, and will contrast them for the four regions.

Acknowledgments. This study was supported by Grant NA07OAR4310495 from the National Oceanic and Atmospheric Administration/Climate and Global Change Program Climate Prediction Program for the Americas (NOAA/CPPA). We appreciate the comments of Dr. Brant Liebmann and two anonymous reviewers, which led to significant improvements in the presentation of the results.

REFERENCES

Adler, R. F., and Coauthors, 2003: The version-2 Global Precipitation Climatology Project (GPCP) monthly precipitation analysis (1979–present). *J. Hydrometeor.,* **4,** 1147–1167.

Andreae, M. O., D. Rosenfeld, P. Artaxo, A. Costa, G. Frank, K. Longo, and M. A. F. Silva Dias, 2004: Smoking rain clouds over the Amazon. *Science,* **303,** 1337, doi:10.1126/science.1092779.

Artaxo, P., and Coauthors, 2002: Physical and chemical properties of aerosols in the wet and dry season in Rondonia, Amazonia. *J. Geophys. Res.,* **107,** 8081, doi:10.1029/2001JD000666.

Carvalho, L. M. V., C. B. Jones, and B. Liebmann, 2002: Extreme precipitation events in southern South America and large-scale convective patterns in the South Atlantic convergence zone. *J. Climate,* **15,** 2377–2394.

——, ——, and ——, 2004: The South Atlantic convergence zone: Intensity, form, persistence, relationships with intraseasonal to interannual activity, and extreme rainfall. *J. Climate,* **17,** 88–108.

Christian, H., and Coauthors, 2003: Global frequency and distribution of lightning as observed from space by the Optical Transient Detector. *J. Geophys. Res.,* **108,** 4005, doi:10.1029/2002JD002347.

Cooke, W., and J. Wilson, 1996: A global black carbon aerosol model. *J. Geophys. Res.,* **101** (D14), 19 395–19 409.

Cotton, W. R., M. Lin, R. McAnelly, and C. Tremback, 1989: A composite model of mesoscale convective complexes. *Mon. Wea. Rev.,* **117,** 765–783.

DeMott, C. A., and S. Rutledge, 1998: The vertical structure of TOGA COARE convection. Part I: Radar echo distributions. *J. Atmos. Sci.,* **55,** 2730–2747.

Durkee, J. D., and T. L. Mote, 2009: A climatology of subtropical South American mesoscale convective complexes. *Int. J. Climatol.,* **30** (3), 418–431.

——, ——, and J. M. Shepherd, 2009: The contribution of mesoscale convective complexes to rainfall across subtropical South America. *J. Climate,* **22,** 4590–4605.

Fisch, G., J. Tota, L. A. T. Machado, M. A. F. Silva Dias, R. F. da F. Lyra, C. Nobre, A. Dolman, and J. Gash, 2004: The convective boundary layer over pasture and forest in Amazonia. *Theor. Appl. Climatol.,* **78,** 47–59, doi:10.1007/s00704-004-0043-x.

Freitas, S., and Coauthors, 2005: Monitoring the transport of biomass burning emissions in South America. *Environ. Fluid Mech.,* **5,** 135–167.

Fu, R., and W. Li, 2004: The influence of the land surface on the transition from dry to wet season in Amazonia. *Theor. Appl. Climatol.,* **78,** 97–110, doi:10.1007/s00704-004-0043-x.

——, B. Zhu, and R. E. Dickinson, 1999: How do atmosphere and land surface influence seasonal changes of convection in the tropical Amazon? *J. Climate,* **12,** 1306–1321.

Garreaud, R. D., 2000: Cold air intrusions over subtropical South America: Structure and dynamics. *Mon. Wea. Rev.,* **128,** 2544–2599.

Gonzalez, M., C. Vera, B. Liebmann, J. Marengo, V. Kousky, and D. Allured, 2007: The nature of the rainfall onset over central South America. *Atmósfera,* **20,** 377–394.

Holton, J. R., 2004: *An Introduction to Dynamic Meteorology*. 4th ed. Academic Press, 535 pp.

Horel, J. D., A. Hahmann, and J. Geisler, 1989: An investigation of the annual cycle of convective activity over the tropical Americas. *J. Climate,* **2,** 1388–1403.

Houze, R. A., 1989: Observed structure of mesoscale convective systems and implications for large-scale heating. *Quart. J. Roy. Meteor. Soc.,* **115,** 425–461.

Jones, C. B., and L. M. V. Carvalho, 2002: Active and break periods in the South America monsoon system. *J. Climate,* **15,** 905–914.

Kalnay, E., and Coauthors, 1996: The NCEP/NCAR 40-Year Reanalysis Project. *Bull. Amer. Meteor. Soc.,* **77,** 437–472.

Keenan, T. D., and R. Carbone, 1992: A preliminary morphology of precipitation systems in tropical northern Australia. *Quart. J. Roy. Meteor. Soc.,* **118,** 283–326.

Kousky, V. E., 1988: Pentad outgoing longwave radiation climatology for the South American sector. *Rev. Bras. Meteor.,* **3,** 217–231.

Laing, A. G., and J. M. Fritsch, 1997: The global population of mesoscale convective complexes. *Quart. J. Roy. Meteor. Soc.,* **123,** 389–405.

Liebmann, B., G. N. Kiladis, J. A. Marengo, T. Ambrizzi, and J. D. Glick, 1999: Submonthly convective variability over South America and the South Atlantic convergence zone. *J. Climate,* **12,** 1877–1891.

——, ——, C. S. Vera, A. C. Saulo, and L. M. V. Carvalho, 2004: Subseasonal variations of rainfall in South America in the vicinity of the low-level jet east of the Andes and comparison to those in the South Atlantic convergence zone. *J. Climate,* **17,** 3829–3842.

Maddox, R. A., 1980: Mesoscale convective complexes. *Bull. Amer. Meteor. Soc.,* **61,** 1374–1387.

Marengo, J. A., B. Liebmann, V. E. Kousky, N. P. Filizola, and I. Wainer, 2001: Onset and end of the rainy season in the Brazilian Amazon basin. *J. Climate,* **14,** 833–852.

——, W. Soares, C. Saulo, and M. Nicolini, 2004: Climatology of the low-level jet east of the Andes as derived from the NCEP–NCAR reanalyses: Characteristics and temporal variability. *J. Climate,* **17,** 2261–2280.

Mohr, K. I., and E. J. Zipser, 1996: Mesoscale convective systems defined by their 85-GHz ice scattering signature: Size and intensity comparison over tropical oceans and continents. *Mon. Wea. Rev.,* **124,** 2417–2437.

Nesbitt, S. W., E. J. Zipser, and D. J. Cecil, 2000: A census of precipitation features in the tropics using TRMM: Radar, ice scattering, and lightning observations. *J. Climate,* **13,** 4087–4106.

——, R. Cifelli, and S. Rutledge, 2006: Storm morphology and rainfall characteristics of TRMM precipitation features. *Mon. Wea. Rev.,* **134,** 2702–2721.

Nieto-Ferreira, R., and T. M. Rickenbach, 2010: Regionality of monsoon onset in South America: A three-stage conceptual model. *Int. J. Climatol.,* in press, doi:10.1002/joc.2161.

Nogues-Paegle, J. N., and K. C. Mo, 1997: Alternating wet and dry conditions over South America during summer. *Mon. Wea. Rev.,* **125,** 279–291.

Petersen, W., and S. Rutledge, 2001: Regional variability in tropical convection: Observations from TRMM. *J. Climate,* **14,** 3566–3586.

Potter, C., V. Brooks-Genovese, S. Klooster, M. Bobo, and A. Torregrosa, 2001: Biomass burning losses of carbon estimated from ecosystem modeling and satellite data analysis for the Brazilian Amazon region. *Atmos. Environ.,* **35,** 1773–1781.

Rickenbach, T. M., R. Nieto Ferreira, J. Halverson, D. Herdies, and M. A. F. Silva Dias, 2002: Modulation of convection in the southwestern Amazon basin by extratropical stationary fronts. *J. Geophys. Res.,* **107,** 8040, doi:10.1029/2000JD000263.

Salati, E., and P. B. Vose, 1984: Amazon Basin: A system in equilibrium. *Science,* **225,** 129–138, doi:10.1126/science.225.4658.129.

Velasco, I., and M. Fritsch, 1987: Mesoscale convective complexes in South America. *J. Geophys. Res.,* **92** (D8), 9591–9613.

Williams, E. R., M. E. Weber, and R. E. Orville, 1989: The relationship between lightning type and convective state of thunderclouds. *J. Geophys. Res.,* **94** (D11), 13 213–13 220.

——, and Coauthors, 2002: Contrasting convective regimes over the Amazon: Implications for cloud electrification. *J. Geophys. Res.,* **107,** 8082, doi:10.1029/2001JD000380.

Zhou, J., and K. M. Lau, 1998: Does a monsoon climate exist over South America? *J. Climate,* **11,** 1020–1040.

Zipser, E. J., and K. Lutz, 1994: The vertical profile of radar reflectivity of convective cells: A strong indicator of storm intensity and lightning probability? *Mon. Wea. Rev.,* **122,** 1751–1759.

——, D. J. Cecil, C. Liu, S. W. Nesbitt, and D. P. Yorty, 2006: Where are the most intense thunderstorms on Earth? *Bull. Amer. Meteor. Soc.,* **87,** 1057–1071.